

A Variable-speed Control Method to Reduce Ducted-fan Thrust Fluctuations for Flying Car Utilization

Y. W. Luo, Y. H. He, Y. P. Qian[†] and Y. J. Zhang

State Key Laboratory of Intelligent Green Vehicle and Mobility, School of Vehicle and Mobility, Tsinghua University, Beijing, China

[†]Corresponding Author Email: qianyuping@tsinghua.edu.cn

ABSTRACT

Flying cars, or vertical takeoff and landing (VTOL) aircraft, are revolutionary devices that can address traffic congestion and help build a three-dimensional transportation system in the future. Flight safety could deteriorate in actual flight because ducted fans may suffer from significant thrust fluctuations induced by crosswinds. In this article, we propose a variable-speed control method to reduce thrust fluctuations by applying a speed waveform opposite to the fluctuation waveform. We choose a typical condition of a 5 m/s crosswind for validation. The results of unsteady Reynolds averaged Navier–Stokes (URANS) calculations show that crosswinds lead to fluctuations in all thrusts with the frequency of the blade passing frequency. The total thrust fluctuation amplitude accounts for 6.2% of the total thrust. By applying the variable-speed control where the frequency is identical to the thrust fluctuation frequency, the phase difference is 180 degrees, and the amplitude is approximately the square root of the fluctuation amplitude, the standard deviation of the thrust fluctuation is reduced by 92% without affecting the mean total thrust. Fluctuations in other performance parameters, such as lateral force and pitching moment, are improved as well. This active control method can achieve accurate control without any auxiliary equipment and has good application prospects. It provides a promising idea for solving the problem of performance fluctuations in turbomachinery.

Article History

Received December 25, 2023

Revised February 28, 2024

Accepted April 18, 2024

Available online July 31, 2024

Keywords:

Flying car

Ducted fan

Thrust fluctuation

Crosswind

Speed control

1. INTRODUCTION

Flying cars (Luo et al., 2021; Liu et al., 2022), as shown in Fig. 1, are a revolutionary way to address traffic congestion and help build a three-dimensional transportation system in the future. This is expected to reshape future transportation modes (Liu et al., 2023). Compared with traditional means of transportation, flying can provide fast point-to-point transportation services. For example, there is a classic case described by Uber in which a flying car can shorten the journey from San Francisco's wharf to downtown San Jose to 15 minutes, which usually takes 2 hours in an ordinary car (Elevate, 2016). The advantages of being convenient, time-saving, and safe make it the most ideal choice for urban air mobility (UAM). Flying cars have therefore attracted the attention of many companies and researchers (Ahmed et al., 2020; Swaminathan et al., 2022).

A ducted fan is a potential propulsion unit for flying cars that offers high safety, high efficiency, and minimal



Fig. 1 Ducted-fan flying car

noise (Qian et al., 2022; Jin et al., 2023; Li et al., 2023; Li & Liu, 2023). The surrounding environment is likely to cause aerodynamic interference to a ducted fan during operation and could lead to a shift in performance (Luo et al., 2023a; Xv et al., 2023). Severe performance degradation may even cause the flying car to lose control (Luo et al., 2023b; Wang et al., 2023). Among several

NOMENCLATURE			
ρ	air density	C_T	thrust coefficient
A	disk area	C_Q	torque coefficient
Ω	rotating speed	C_X	lateral force coefficient
R	rotor radius	C_M	pitching moment coefficient
T	thrust	B	variable-speed amplitude
Q	torque	ω	variable-speed frequency
F_x	lateral force	φ	variable-speed phase
M_z	pitching moment	k	mean rotating speed

operating conditions, flying in crosswinds is one of the most typical and dangerous scenarios (Ai et al., 2020; Zhao et al., 2022, 2023). The capital of China, Beijing, frequently experiences severe gusts that can reach 30 m/s despite the annual average wind speed being less than 4 m/s (Shi et al., 2019). Strong winds are a major obstacle to the operation of ducted fans. Thus, it is crucial to improve the performance with effective control methods. There have been numerous studies on ducted fans operating under wind conditions. Some researchers have employed computational and experimental methods to explore aerodynamic performance. Martin and Tung (2004) carried out a wind tunnel test to analyze the ducted fan performance for hovering in open space and in crosswinds. They found that a duct shape with a small leading-edge radius could improve the pitching moment during stall. Ryu et al. (2016) conducted RANS calculations to analyze the influence of crosswinds at different speeds and in different directions on the ducted fan characteristics. A wind tunnel test was carried out for validation. The researchers noted that the pitching moment must be reduced in crosswinds since it was significantly affected by the asymmetric thrust generated by the difference in airflow velocity at the duct lip section.

Other researchers have proposed novel designs or active control strategies for crosswind performance improvement. Camci and Akturk (2010; 2016) designed a double-ducted fan (DDF), a device that adds a second duct to eliminate lip flow separation. They noted that a DDF could lead to thrust enhancement, nose-up pitching moment control, and recovery of the mass flow rate through the rotor disk in a wide horizontal flight range. Ohanian et al. (2011) investigated new uses of synthetic jet actuators in ducted fans. Synthetic jets can produce control forces and moments to counteract outside interference. They found that synthetic jets could successfully produce the same duct leading-edge separation as steady jets at a much lower blowing rate.

Previous studies have focused mainly on the stability problem in crosswinds, especially the pitching moment. However, our recent studies revealed that crosswinds can have significant unsteady effects in addition to steady effects on the aerodynamic force and moment (Luo et al., 2024). The thrust of a ducted fan fluctuates due to the circumferential asymmetry induced by the crosswind, the amplitude of which increases remarkably with the wind speed. Flow instability might even occur under high-speed wind conditions. Thrust fluctuations pose a serious challenge to accurate flight control and need to be dealt

with properly for better stability. Past studies make no contribution to this topic.

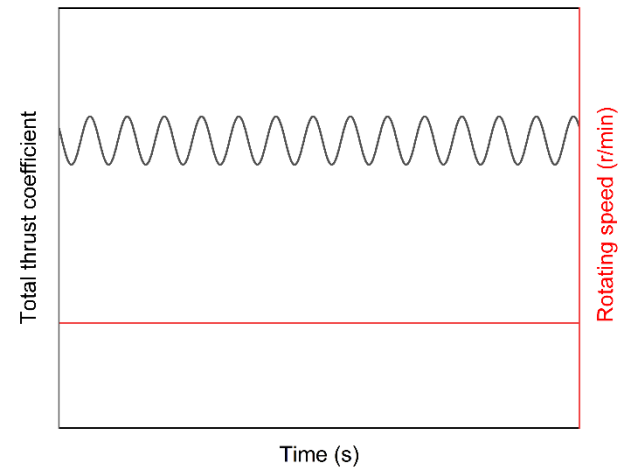
In this paper, we propose a novel variable-speed control method for suppressing thrust fluctuations in ducted fans under crosswind conditions. The fundamental idea is to apply a designed speed waveform opposite to the fluctuation waveform to offset the thrust fluctuation. Based on a URANS model, we choose a typical crosswind condition and carry out a numerical simulation for method validation. The contribution of this work lies in that we verify the feasibility of the variable-speed control method in principle and discuss the influence of three key parameters in detail. We hope that the obtained results can provide a useful reference for suppressing the performance fluctuations of ducted fans and can even be applied to other turbomachinery for performance improvement.

The remaining sections of the paper is structured as follows: Section 2 describes the principle of the variable-speed control method. Section 3 introduces a test case for method validation, where the adopted CFD methods are given, and an optimal control strategy is constructed based on the results of parameter sensitivity analysis. Section 4 draws the conclusions.

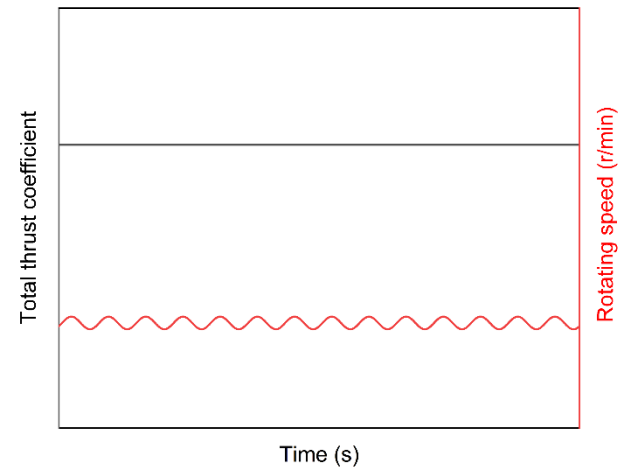
2. METHOD DESCRIPTION

The proposed variable-speed control method is illustrated in Fig. 2. A ducted fan can usually provide stable thrust at a constant rotating speed in the absence of external interference. However, due to the circumferential asymmetry effect caused by unilateral wind, the blade angle of attack and airflow velocity vary with circumferential angle, which leads to sinusoidal changes in thrust during fan rotation, as shown in Fig. 2(a). The sine frequency is equal to the blade passing frequency since a multiblade ducted fan will achieve the same position in space for every certain degree.

A sinusoidal change in the ducted fan thrust during static hover can be realized by applying a sine-varying rotating speed waveform. This point is instructive and can be applied to crosswind conditions to solve the thrust fluctuation problem. We deduce that if the frequency, amplitude, and phase of the rotating speed are properly set, the sine-varying waveform can, in principle, offset the asymmetric effect induced by the crosswind. The thrust fluctuations are precisely and effectively reduced, as shown in Fig. 2(b).



(a) Constant rotating speed



(b) Variable rotating speed

Fig. 2 Principle diagram of variable speed control

3. TEST CASE

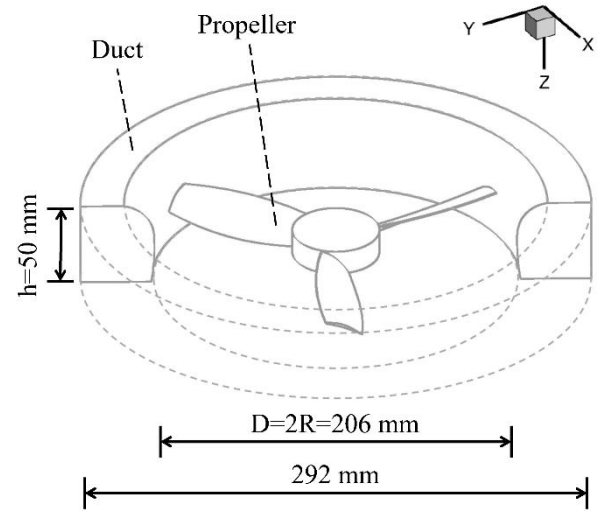
In this section, the ability of the proposed variable-speed control method to reduce ducted-fan thrust fluctuations is verified through three-dimensional numerical simulation using a typical case of hovering in a 5 m/s crosswind. We first introduce the adopted CFD model for subsequent investigations and its corresponding experimental validation. We then study the influence of three parameters—phase, amplitude, and frequency—on the degree of thrust fluctuation suppression. Finally, we comprehensively compare the ducted fan aerodynamic performance with and without the optimal strategy to illustrate the effectiveness of the proposed method.

In this paper, the dimensionless mechanical parameters for result analysis are collected and defined as follows:

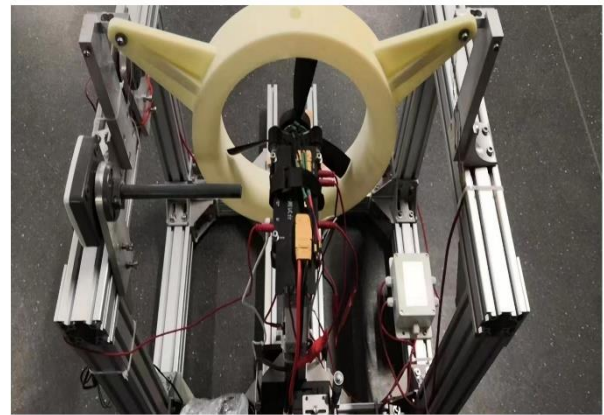
Thrust coefficient:

$$C_T = \frac{T}{\rho A \Omega^2 R^2} \quad (1)$$

Torque coefficient:



(a) Ducted fan geometry



(b) Test bench

Fig. 3 Configurations of the investigated ducted fan

$$C_Q = \frac{Q}{\rho A \Omega^2 R^3} \quad (2)$$

Lateral force coefficient:

$$C_x = \frac{F_x}{\rho A \Omega^2 R^2} \quad (3)$$

Pitching moment coefficient:

$$C_M = \frac{M_z}{\rho A \Omega^2 R^3} \quad (4)$$

where R refers to the rotor radius, Ω refers to the rotating speed, A refers to the rotor disk area, and ρ refers to the air density.

3.1 Numerical Setup

Figure 3(a) shows the detailed structure of the studied ducted fan. The ducted fan consists of two parts, a duct and a propeller. The propeller is shrouded by the duct and

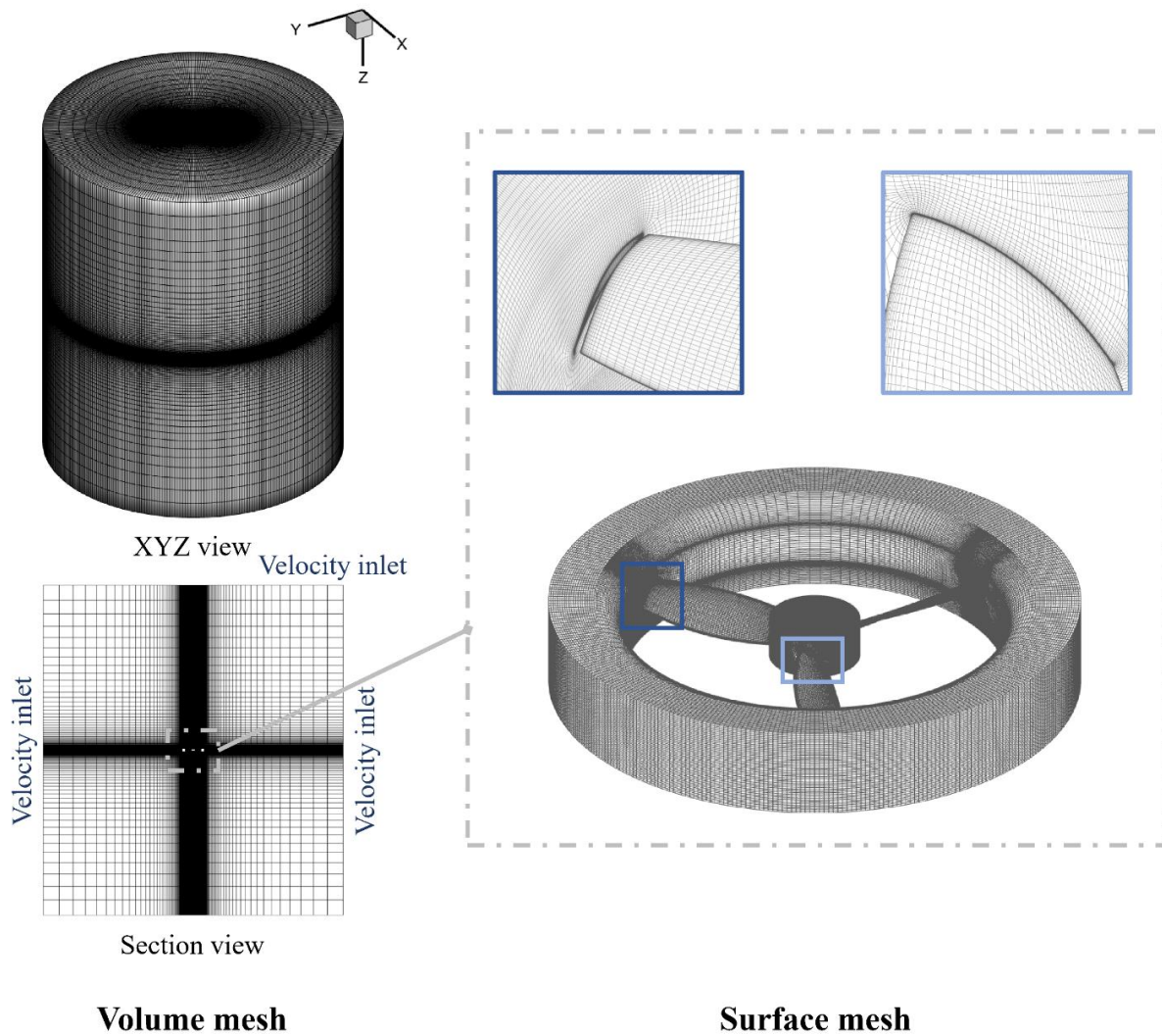


Fig. 4 Structured mesh details in the numerical setup

has three equally distributed blades with a diameter of 206 mm. The duct is a short-type duct with a height of 50 mm and a diameter of 292 mm. This ducted fan could be widely used in flying cars for urban transportation due to its light structure and minimal air drag. Figure 3(b) shows a photograph of the ducted fan arranged on the test bench.

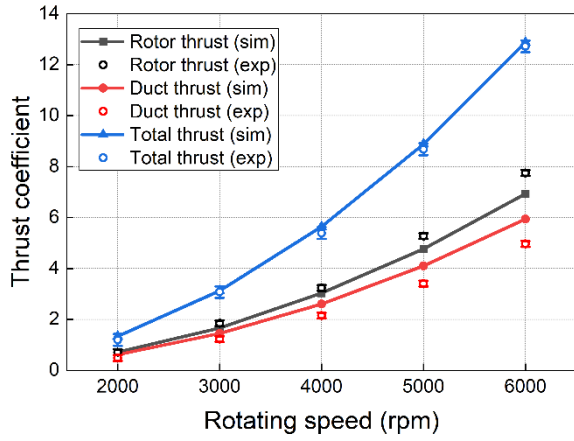
Regarding the numerical setup, Fig. 4 depicts the overall computational domains along with the mesh grids. We separated the domains into two categories. The static domain was a cylinder for simulating the external flow field. It had a diameter of 40R and a height of 47R. Hexahedral structured grids in the static domain were generated in ANSYS ICEM CFD. By controlling the exponential distribution of nodes from near to far away from the ducted fan, we improved the calculation accuracy of the surrounding physical field and avoided the unnecessary consumption of computing resources. The worst mesh quality was above 0.7. The rotating domain was the inner region inside the duct. It rotates at the same speed as the ducted fan. The structured grids in the rotating domain were generated based on NUMECA AutoGrid 5. There were a total of 17 boundary layers on the rotor surface. The volume mesh had a minimum skewness of

more than 19, a maximum aspect ratio of almost 600, and a maximum expansion ratio of 3.85. Figure 4(b) shows the surface mesh and highlights the grids in key flow regions, including the tip region and the hub region. Overall, there were roughly a total of 12 million grids for computation, with each domain comprising half. High-quality grids have laid a solid foundation for accurate prediction of the ducted fan aerodynamic performance.

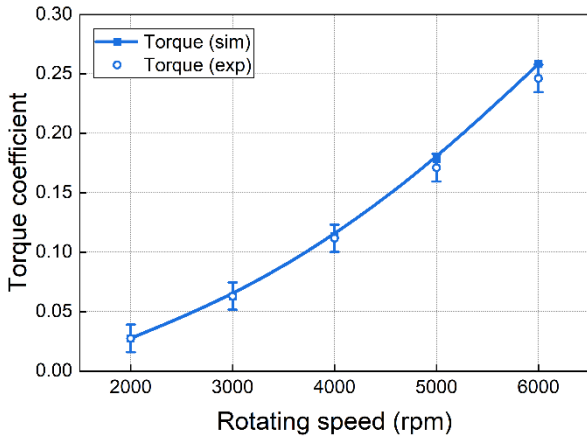
The commercial tool ANSYS Fluent served as the basis for the numerical simulation. A pressure-based solver was used since the compressibility of gas can be ignored with a maximum Mach number close to 0.1. Without the body force and gravity term, the Navier-Stokes equations are

$$\frac{\partial u_i}{\partial x_i} = 0 \quad (5)$$

$$\frac{\partial(\rho u_i)}{\partial t} + \frac{\partial(\rho u_i u_j)}{\partial x_j} = -\frac{\partial p}{\partial x_i} + \frac{\partial}{\partial x_j} \left[\mu \left(\frac{\partial u_i}{\partial x_j} + \frac{\partial u_j}{\partial x_i} \right) \right] \quad (6)$$



(a) Thrust performance



(b) Torque performance

Fig. 5 Comparison between the test data and the computational results

where μ represents the air dynamic viscosity, u_i represents the velocity vector, and p represents the pressure.

The shear stress transport (SST) $k-\omega$ turbulence model was used to solve the transport equations in the RANS model, where the turbulence kinetic energy k and specific dissipation rate ω are given by

$$\frac{\partial(\rho k)}{\partial t} + \frac{\partial(\rho k u_i)}{\partial x_j} = \frac{\partial}{\partial x_j} \left[\left(\mu + \frac{\mu_t}{\sigma_k} \right) \frac{\partial k}{\partial x_j} \right] + P_k - D_k + S_k \quad (7)$$

$$\frac{\partial(\rho \omega)}{\partial t} + \frac{\partial(\rho \omega u_i)}{\partial x_j} = \frac{\partial}{\partial x_j} \left[\left(\mu + \frac{\mu_t}{\sigma_\omega} \right) \frac{\partial \omega}{\partial x_j} \right] + P_\omega - D_\omega + S_\omega \quad (8)$$

where σ_k and σ_ω are the turbulent Prandtl numbers of k and ω , P_k and P_ω are turbulent energy generation terms, D_k and D_ω are dissipation terms, and S_k and S_ω are user-defined source terms.

The coupled solution algorithm was used to improve the robustness of the computational calculations. The second-order upwind scheme was used for better

Table 1 Grid convergence test results for a ducted fan in hover mode ($\Omega = 4000$ r/min)

Cell number	Total thrust (N)	Relative error (%)
6 million	5.4695	2.96
9 million	5.5946	0.74
12 million	5.6363	0

accuracy. Figure 4(a) shows the boundary conditions. The outside boundary of the static domain was velocity inlet, where relevant parameters were adjusted in different cases. Two pairs of interfaces were created between the rotating and static domains to guarantee data transmission. The inner duct in the rotating domain was configured as a stationary wall, while the rest were kept as nonslip walls.

For validation purposes, we conducted bench tests on the investigated ducted fan at the Chongqing Innovation Center of the Beijing Institute of Technology and compared the bench test results and simulation results, as shown in Fig. 5. Our adopted CFD method could predict the ducted fan aerodynamics well, with errors of thrust and torque predictions lower than 10%. This well-matched result is reasonable considering that the aluminum alloy bracket and sensors for testing may interfere with the ducted fan. In addition, we modified the mesh node distributions to carry out the mesh convergence test. Three mesh qualities with cell numbers ranging from 6 million to 12 million were compared. Table 1 shows the results. Compared with the finest grid, the relative calculation errors obtained with the coarse grid and medium grid were 2.96% and 0.74%, respectively. The medium-quality mesh and fine-quality mesh were adequate to ensure the calculation accuracy. We chose a fine mesh with 12 million volume grids for subsequent investigation of our proposed control method.

3.2 Performance Without Control

Figure 6 shows the typical and distinctive thrust properties of a ducted fan operating at constant rotating speeds under wind conditions. The crosswind speed is 5 m/s, and the rotating speed of the ducted fan is fixed at 4000 r/min. The rotor thrust, which makes up roughly 60% of the total thrust, is the primary contributor. All the thrusts vary sinusoidally with time. The thrust fluctuation frequency is 200 Hz, which equals the blade passing frequency. The total thrust fluctuation amplitude, which accounts for 6.2% of the mean total thrust, is the highest, with a major contribution from rotor thrust fluctuations and a minor contribution from duct thrust fluctuations.

An analysis of the fan positions revealed that the total thrust increases from State 1 to State 2 and decreases from State 2 to State 3 during a cycle. State 2 achieves the greatest thrust, while States 1 and 3 have the minimal thrust. This rule is basically true of other crosswind conditions, despite different thrust fluctuation amplitudes.

The velocity magnitude contours are shown in Fig. 7. Cases with crosswind speeds of 0 m/s and 5 m/s are compared. When the ducted fan hovers in the open space, as shown in Fig. 7(a), the rotating fan draws air from the open atmosphere and accelerates it to form a downward

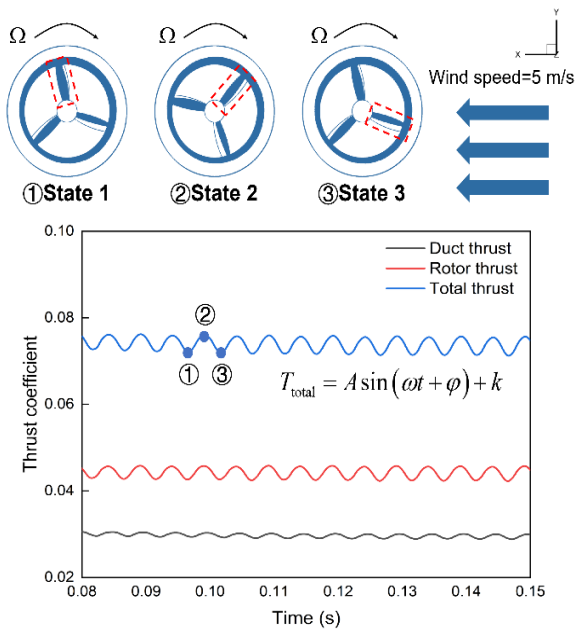


Fig. 6 Typical diagram of the ducted fan performance under a 5 m/s crosswind

wake. There exist significant flow separations at the diffuser section. When the ducted fan hovers in 5 m/s wind, which is shown in Fig. 7(b), the crosswind causes the streamlines to tilt from upwind to downwind, resulting in contraction of the wake. The mass flow rate through the rotor disk decreases because significant wake contraction reduces the effective flow area. Under this circumstance, the upwind flow separations, particularly those at the

diffuser, are improved, while the downwind flow separation of the duct vanishes. Newly generated significant flow separation also shows up at the outside duct in the downwind.

To study the flow asymmetry induced by the crosswind, Fig. 8 shows the static pressure distribution on the ducted fan surface. In terms of the duct performance, the crosswind leads to opposite pressure distributions. On the upwind side, there is an obvious low-pressure region formed at the lip due to flow separation, while there is relatively high pressure at the bottom of the duct. The pressure difference between the upper surface and lower surface has a positive effect on the duct thrust. In contrast, a high-pressure region is formed at the duct lip of the downwind side due to the impact of airflow, while a low-pressure region is formed at the bottom due to significant flow separation. Therefore, the pressure difference has a negative effect on the duct thrust in the downwind.

For the rotor performance, the fan blade thrust is unevenly distributed on the circumference, which varies with the azimuth angle. According to the lift formula, the local air velocity magnitude and the angle of attack are key factors influencing the blade thrust. When the direction of the blade linear velocity is opposite to the crosswind direction, such as for blade 1, the pressure side of the blade forms a large high-pressure region due to increasing angle of attack and local airflow velocity. At this point, the blade thrust remains high. When the linear velocity and crosswind direction are the same, however, a small local airflow velocity and angle of attack cause the high-pressure region on the pressure side to shrink. The blade thrust decreases consequently.

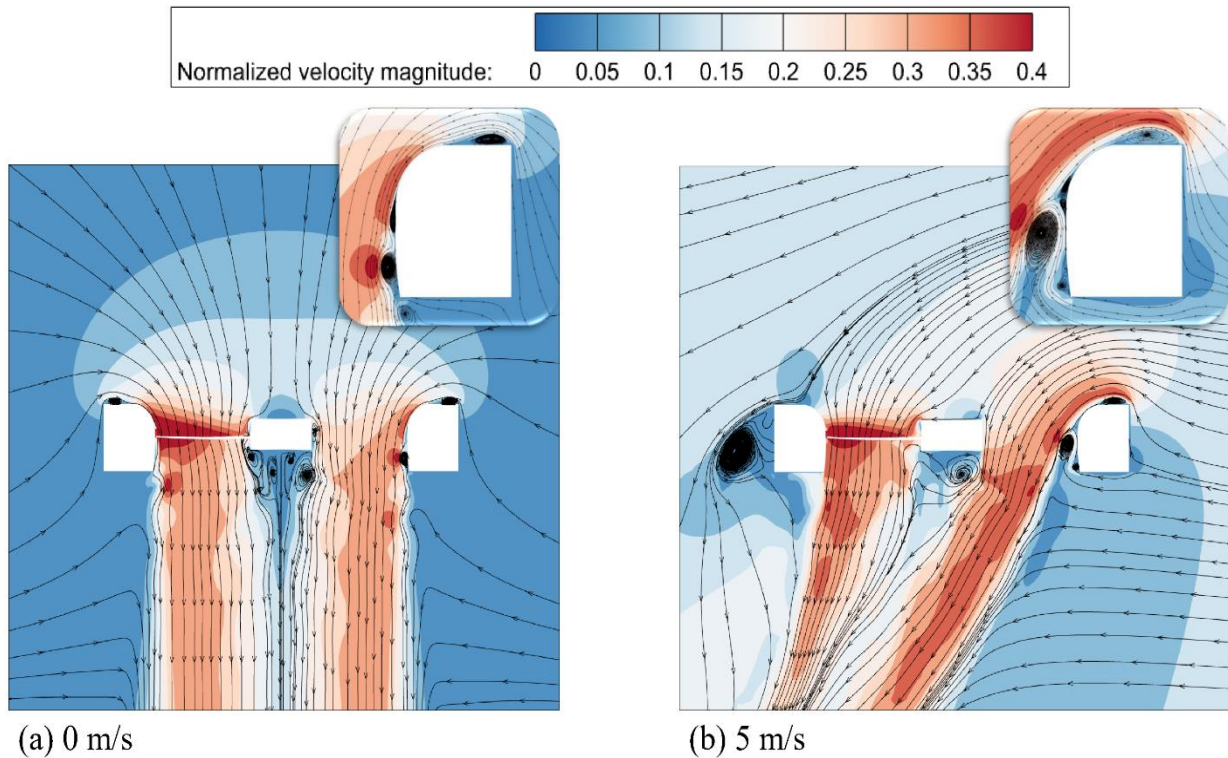


Fig. 7 Velocity magnitude contours for different cases at $\Omega = 4000$ r/min

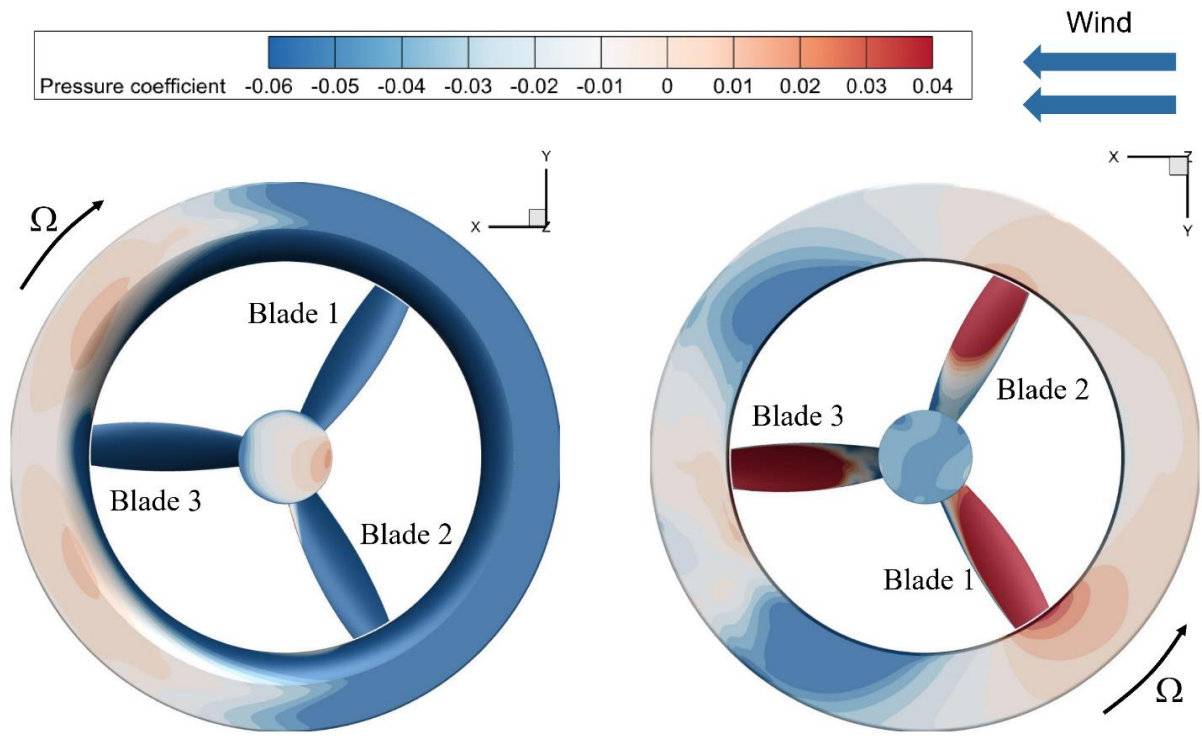


Fig. 8 Static pressure contours on the ducted fan surface under a 5 m/s crosswind

3.3 Performance with Control

In Fig. 6, the relationship between the total thrust and time can be described by the following equation:

$$C_{T_{total}} = B_0 \sin(\omega_0 t + \varphi_0) + k_0 \quad (9)$$

where $B_0 = 0.00259$, $\omega_0 = 400\pi$, $\varphi_0 = 150^\circ$, and $k_0 = 0.07394$. We consider the following rotating speed waveform to suppress the thrust fluctuation:

$$\Omega = B \sin(\omega t + \varphi) + k \quad (10)$$

where B is the amplitude, ω is the frequency, φ is the phase, and k is the mean rotating speed, which is 4000 r/min in all subsequent cases studied.

(a) Effect of the variable-speed phase angle

To investigate the impact of the rotational speed phase on the control performance, we changed the phase from -180° to 180° with an interval of 60° . The relative phase is defined as the difference between φ and $\varphi_0 + 180^\circ$. The fluctuation amplitude B/k is fixed at 1%, and the frequency ω is fixed at 400π . The results are shown in Fig. 9, where the thrust fluctuation is characterized by the standard deviation of the time series data. It is clear that the phase has nothing to do with the ducted-fan mean total thrust but affects the fluctuation amplitude. The minimum thrust fluctuation occurs at the relative phase of 0° , and the fluctuation increases as the phase increases to 180° . The minimum standard deviation at 0° only accounts for 14%

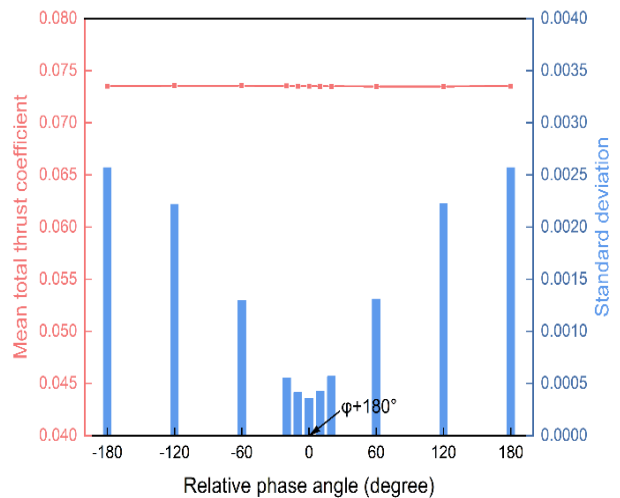


Fig. 9 Effect of variable-speed control under different phase angles

of the maximum standard deviation at 180° . This result is reasonable because, in theory, the sinusoidal thrust with time can be offset most effectively by a sinusoidal rotating speed with a phase difference of 180° . In addition, it can be inferred that an improper phase (i.e., the absolute value of the relative phase is greater than 60° here) would lead to more severe thrust fluctuations because the standard deviation without variable-speed control is 0.00151. This shows that for actual operations, it is crucial to determine the relative angle between the ducted fan blade and the crosswind for the successful implementation of variable-speed control; otherwise, it may lead to the opposite results.

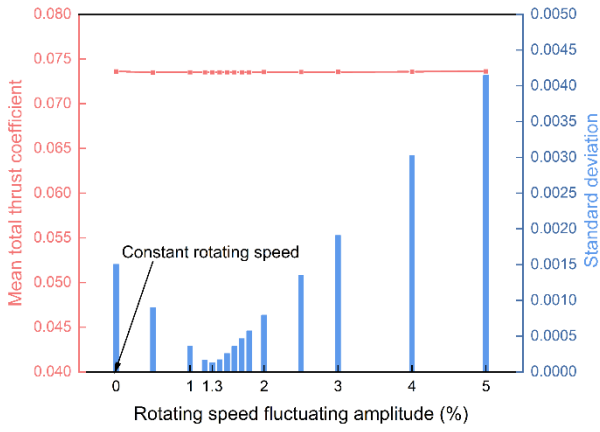


Fig. 10 Effect of variable-speed control under different amplitudes

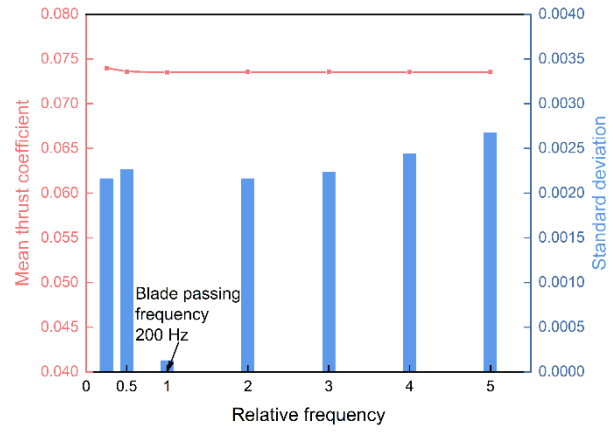


Fig. 11 Effect of variable-speed control under different frequencies

(b) Effect of variable-speed amplitude

Figure 10 shows the effect of the variable-speed amplitude, where the amplitude B is normalized by the mean rotating speed $k = 4000$. The fluctuating amplitude of the rotating speed changes from 0 to 5%, while the relative phase is 150° , and the frequency ω is 400π .

The maximum amplitude of the total thrust fluctuation at a constant speed of 4000 r/min is approximately 3%. In view of the relationship between the rotating speed and thrust, the most effective rotating speed fluctuation in theory should be approximately 1.7%. The actual results are basically consistent with the theory. As shown in Fig. 10, the thrust fluctuation decreases first and then increases with increasing rotating speed fluctuation amplitude. The minimum value appears at 1.3%. When the fluctuation amplitude increases from 0 to 1.3%, the variable-speed control has an inhibitory effect on the thrust fluctuation induced by the crosswind, and the effect is greatly enhanced with increasing fluctuation amplitude. When the fluctuation amplitude is greater than 1.3%, however, the speed control completely suppresses the thrust fluctuation caused by the crosswind and begins to cause additional thrust fluctuations. When the fluctuation amplitude exceeds 2.5%, the thrust fluctuation from the speed control exceeds the original fluctuation from the crosswind. The variable-speed control method is no longer effective under these circumstances.

On the whole, the amplitude of the variable-speed control can effectively adjust the amplitude of the ducted-fan thrust fluctuation while keeping the average total thrust unchanged. However, it is worth noting that the amplitude of the variable-speed control needs to be perfectly matched with the thrust fluctuation to achieve the best control effect.

(c) Effect of variable-speed frequency

Figure 11 focuses on the effect of the variable-speed frequency. The frequency ω is normalized by the thrust fluctuation frequency $\omega_0 = 400\pi$. Cases with different normalized frequencies ranging from 0.5 to 5 are studied for comparison, where the relative phase is fixed at 150° and the relative amplitude is fixed at 1.3%.

Table 2 Comparison of the parameters between the thrust fluctuation and the optimal control method

Parameters	Thrust fluctuation	Speed control
Frequency (Hz)	200	200
Amplitude (%)	3	1.3
Phase (degree)	150	150+180

Similar to the amplitude and phase, the frequency has no marked effect on the mean total thrust. As far as the fluctuation is concerned, the figure shows that only when the variable-speed frequency is equal to the thrust fluctuation frequency induced by the crosswind does the variable-speed control clearly have a negative effect on the thrust fluctuations. In other cases, the thrust fluctuation is greater than that without speed control.

3.4 Discussion

Based on the above research on the three key parameters, we can summarize the characteristics of thrust fluctuation and the applied variable-speed control, as shown in Table 2. Generally, optimal variable-speed control can be achieved by ensuring that the frequency is identical to the thrust fluctuation frequency, the phase difference is 180 degrees, and the amplitude is approximately the square root of the fluctuation amplitude.

Figure 12 shows the time series of the total thrust with and without speed control. Our proposed variable-speed control method greatly suppresses the thrust fluctuations. The range of the thrust fluctuation is reduced by 88%, and the standard deviation of the thrust fluctuation is reduced by 92% under the optimal control strategy. The fundamental frequency component of the thrust fluctuation of 200 Hz is eliminated by the control method, and the remaining component is the double-frequency component. We may take a step to further eliminate the fluctuation if we add a waveform of 400 Hz to the currently existing control waveform.

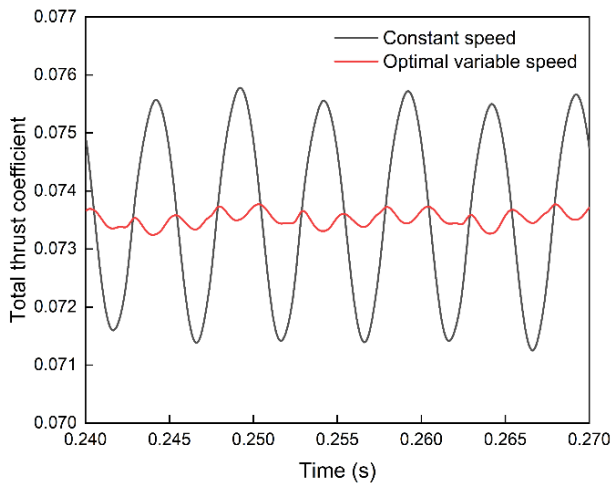


Fig. 12 Comparison of the total thrust performance with and without variable-speed control

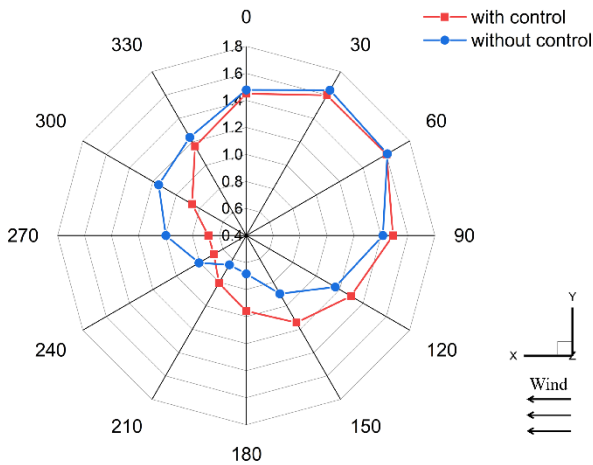


Fig. 13 Comparison of circumferential blade thrust with and without variable-speed control

For the purpose of studying the mechanism of thrust fluctuation optimization, Fig. 13 illustrates the point with the example of rotor thrust. The blade thrust at various circumferential positions with and without variable-speed control is shown for comparison. The blade thrust remains constant during rotation under windless conditions, and the crosswind causes the difference in blade aerodynamic characteristics in the circumferential direction to increase, as shown in Fig. 8. For the case without control, the relative blade tangential velocity increases from 270° to 360° to 90°, while it decreases from 90° to 180° to 270°. The greatest and lowest values occur at 0° and 180°, respectively. However, the flow separation results in a decrease in the mass flow rate and an increase in the angle of attack at upwind side, which is the opposite at downwind side. Thus, the maximum blade thrust appears near 30 degrees, and the minimum blade thrust appears near 210 degrees. The applied control strategy does not change the area encircled by the curve, that is, the mean value of the total thrust, but improves the circumferential distribution of the blade thrust. The thrust distribution becomes more continuous and uniform compared with the

Table 3 Comparisons of performance with and without the variable-speed control method

Performance	Without control (10 ⁻⁴)	With control (10 ⁻⁴)
Blade thrust coef. (mean)	441.1	440.9
Duct thrust coef. (mean)	295.0	294.3
Total thrust coef. (mean)	736.1	735.2
Rotor torque coef. (mean)	149.5	149.5
Lateral force coef. (mean)	109.2	108.4
Pitching moment coef. (mean)	388.8	395.1
Rotor thrust coef. (SD)	11.8	1.8
Duct thrust coef. (SD)	4.0	1.8
Total thrust coef. (SD)	15.1	1.3
Rotor torque coef. (SD)	3.6	1.8
Lateral force coef. (SD)	4.9	4.3
Pitching moment coef. (SD)	14.8	13.9

baseline case, which helps to effectively reduce the total thrust fluctuation of the three blades, although the thrust fluctuation of the single blade is not greatly affected.

Table 3 comprehensively summarizes the aerodynamic performance with and without variable-speed control. The proposed active control strategy does not affect the average aerodynamic performance. It can effectively reduce the total thrust fluctuation from 15.1×10^{-4} to 1.3×10^{-4} , and the fluctuation of the rotor thrust is particularly obvious, from 11.8×10^{-4} to 1.8×10^{-4} . The rotor torque fluctuation is reduced by 50% from 3.6×10^{-4} to 1.8×10^{-4} . In addition, the strategy is beneficial for reducing the fluctuations in the lateral force and pitching moment despite its insignificant effect.

Overall, the variable-speed control method with appropriate parameters can successfully reduce the timing fluctuation of the ducted fan for performance improvement.

4. CONCLUSIONS

Crosswinds are common operating conditions for flying cars. This can introduce significant flow asymmetry and cause tremendous thrust fluctuations in ducted fans, which pose great challenges to flight stability. To solve this problem, we propose a variable-speed control method. The idea is to apply a speed waveform opposite to the fluctuation waveform to offset the thrust fluctuation. We choose a typical crosswind condition for validation, and the results show that our proposed method demonstrates

excellent effectiveness and reliability. The following conclusions are drawn.

For cases without control, the crosswind leads to wake contraction from upwind to downwind. The flow separation near the diffuser at upwind side and that outside the duct at downwind side are enhanced. The crosswind results in different blade thrusts at different circumferential positions. An azimuth angle of 30 degrees corresponds to the maximum blade thrust, while 210 degrees corresponds to the minimum thrust. Meanwhile, the upwind duct thrust stays positive, while the downwind one becomes negative. The thrust fluctuation frequency is identical to the blade passing frequency. The total thrust fluctuation amplitude, which accounts for 6.2% of the mean value, is the greatest, with a major contribution from the rotor and a minor contribution from the duct.

For cases with control, the control effect depends heavily on the control parameters. In terms of the phase, the best control effect occurs for a sinusoidal rotating speed waveform with a phase difference of 180°. The minimum standard deviation is only 14% of the maximum one. In terms of the amplitude, the thrust fluctuation decreases first and then increases with the amplitude of the variable-speed control, and the minimum value appears at 1.3%. The variable-speed control method is no longer effective for amplitudes greater than 2.5% since the thrust fluctuation from the speed control exceeds the original fluctuation from the crosswind. In terms of the frequency, the variable-speed control method is effective in reducing the thrust fluctuation only when the variable-speed frequency is equal to the thrust fluctuation frequency induced by the crosswind.

Overall, current research introduces an active control method for suppressing thrust fluctuations. This method can achieve accurate control without any auxiliary equipment or configurations, which provides a promising idea for solving the problem of performance fluctuations in the field of turbomachinery. However, more cases for validation are needed to comprehensively evaluate the advantages and disadvantages of this strategy. Moreover, owing to the high requirements of the method on the control parameters, more explorations are needed in the future on how to combine the method with the flight controller to improve the stability of the flying car during actual operations.

ACKNOWLEDGMENTS

We would also like to thank Dr. Tianfu Ai and Prof. Bin Xu for their assistance in the experiments.

CONFLICT OF INTEREST

The authors declare no conflicts of interest.

AUTHOR CONTRIBUTIONS

Yiwei Luo: Methodology, Computation, Writing – original draft; **Yuhang He:** Writing – original draft; **Yuping Qian:** Formal analysis; **Yangjun Zhang:** Supervision

REFERENCES

- Ahmed, S. S., Hulme, K. F., Fountas, G., Eker, U., Benedyk, I. V., Still, S. E., & Anastasopoulos, P. C. (2020). The flying car—challenges and strategies toward future adoption. *Frontiers in Built Environment*, 6, 106. <https://doi.org/10.3389/fbuil.2020.00106>
- Ai, T., Xu, B., Xiang, C., Fan, W., & Zhang, Y. (2020). Aerodynamic analysis and control for a novel coaxial ducted fan aerial robot in ground effect. *International Journal of Advanced Robotic Systems*, 17(4), 1729881420953026. <https://doi.org/10.1177/1729881420953026>
- Camci, C. & Aktürk, A. (2010). *Double ducted fan (DDF) as a novel ducted fan inlet lip separation control device*. International Powered Lift Conference.
- Camci, C., & Aktürk, A. (2016). *A VTOL-UAV Inlet flow distorti on reduction concept using a new flow control approach: double-ducted-fan*. 16th International Symposium on Transport Phenomena and Dynamics of Rotating Machinery,
- Elevate, U. (2016). Fast-forwarding to the future of on-demand urban air transportation. <https://www.uber.com/elevate.pdf>
- Jin, Z., Li, D., & Xiang, J. (2023). Robot pilot: a new autonomous system toward flying manned aerial vehicles. *Engineering*. <https://doi.org/10.1016/j.eng.2022.10.018>
- Li, H., Kan, Z., Bie, D., Li, D., & Zhao, S. (2023). Aerodynamic interference analysis of multiple rotors in a heterogeneous unmanned aircraft system. *Physics of Fluids*, 35(11). <https://doi.org/10.1063/5.0174331>
- Li, H., & Liu, K. (2023). Aerodynamic design optimization and analysis of ducted fan blades in DEP UAVs. *Aerospace*, 10(2), 153. <https://doi.org/10.3390/aerospace10020153>
- Liu, M., Hao, H., Lin, Z., He, X., Qian, Y., Sun, X., Geng, J., Liu, Z., & Zhao, F. (2023). Flying cars economically favor battery electric over fuel cell and internal combustion engine. *PNAS nexus*, 2(3), pgad019. <https://doi.org/10.1093/pnasnexus/pgad019>
- Liu, M., Qian, Y., Luo, Y., Hao, H., Liu, Z., Zhao, F., Sun, X., Xun, D., & Geng, J. (2022). Lifecycle greenhouse gas emissions and energy cost analysis of flying cars with three different propulsion systems. *Journal of Cleaner Production*, 331, 129985. <https://doi.org/10.1016/j.jclepro.2021.129985>
- Luo, Y., Ai, T., He, Y., Xu, B., Qian, Y., & Zhang, Y. (2023a). Numerical investigation on unsteady characteristics of ducted fans in ground effect. *Chinese Journal of Aeronautics*. <https://doi.org/10.1016/j.cja.2023.04.004>
- Luo, Y., Ai, T., He, Y., Xu, B., Qian, Y., & Zhang, Y. (2024). Numerical analysis of wind effects on aerodynamic characteristics of a ducted fan. *Chinese*

Journal of Aeronautics.
<https://doi.org/10.1016/j.cja.2024.02.002>

- Luo, Y., Ai, T., He, Y., Zhao, Z., Xu, B., Qian, Y., Peng, J., & Zhang, Y. (2023b). Aerodynamic analysis on unsteady characteristics of a ducted fan hovering in ceiling effect. *Engineering Applications of Computational Fluid Mechanics*, 17(1), 2196327. <https://doi.org/10.1080/19942060.2023.2196327>
- Luo, Y., Qian, Y., Zeng, Z., & Zhang, Y. (2021). Simulation and analysis of operating characteristics of power battery for flying car utilization. *eTransportation*, 8, 100111. <https://doi.org/10.1016/j.etrans.2021.100111>
- Martin, P., & Tung, C. (2004). Performance and flowfield measurements on a 10-inch ducted rotor vtol uav. <https://ntrs.nasa.gov/citations/20050009943>
- Ohanian III, O. J., Karni, E. D., Londenberg, W. K., Gelhausen, P. A., & Inman, D. J. (2011). Ducted-fan force and moment control via steady and synthetic jets. *Journal of Aircraft*, 48(2), 514-526. <https://doi.org/10.2514/1.C031110>
- Qian, Y., Luo, Y., Hu, X., Zeng, Z., & Zhang, Y. (2022). Improving the performance of ducted fans for VTOL applications: a review. *Science China Technological Sciences*, 65(11), 2521-2541. <https://doi.org/https://doi.org/10.1007/s11431-021-2110-x>
- Ryu, M., Cho, L., & Cho, J. (2016). Aerodynamic analysis of the ducted fan for a VTOL UAV in crosswinds. *Transactions of the Japan Society for Aeronautical and Space Sciences*, 59(2), 47-55. <https://doi.org/10.2322/tjsass.59.47>
- Shi, P., Zhang, G., Kong, F., Chen, D., Azorin-Molina, C., & Guijarro, J. A. (2019). Variability of winter haze over the Beijing-Tianjin-Hebei region tied to wind speed in the lower troposphere and particulate sources. *Atmospheric Research*, 215, 1-11. <https://doi.org/10.1016/j.atmosres.2018.08.013>
- Swaminathan, N., Reddy, S. R. P., RajaShekara, K., & Haran, K. S. (2022). Flying cars and evtols—technology advancements, powertrain architectures, and design. *IEEE Transactions on Transportation Electrification*, 8(4), 4105-4117. <https://doi.org/10.1109/TTE.2022.3172960>
- Wang, J., Chen, R., Yu, Z., & Lu, J. (2023). Ground test and numerical investigation on aerodynamic performance of a quad tilt-rotor aircraft in ground and water effects. *Ocean Engineering*, 289, 116169. <https://doi.org/10.1016/j.oceaneng.2023.116169>
- Xv, H., Zhao, L., Wu, M., Liu, K., Zhang, H., & Wu, Z. (2023). Analysis of the impact of structural parameter changes on the overall aerodynamic characteristics of ducted UAVs. *Drones*, 7(12), 702. <https://doi.org/10.3390/drones7120702>
- Zhao, Y., Tian, Y., & Wan, Z. (2022). Aerodynamic characteristics of a ducted fan hovering and transition in ground effect. *Aerospace*, 9(10), 572. <https://doi.org/10.3390/aerospace9100572>
- Zhao, Y., Tian, Y., & Wan, Z. (2023). Longitudinal aerodynamic characteristics of ducted fan propelled fixed-wing VTOL aircraft hovering in ground effect. *Aerospace*, 10(8), 659. <https://doi.org/10.3390/aerospace10080659>